Version of Record: https://www.sciencedirect.com/science/article/pii/S0022311522000897
Manuscript_51a1a26be2fa54f69872228a3276d27a

Mesoscale modeling of microstructure-dependent thermal conductivity in U-Zr fuels

Weiming Chen and Xian-Ming Bai*

Department of Materials Science and Engineering, Virginia Polytechnic Institute and State University, Blacksburg, VA 24061

Abstract

In uranium-zirconium (U-Zr) based metallic fuels, different phases can form at different compositions and temperatures. Typically, lamellar δ-UZr_2 and α-U phases are the dominant microstructures in U-rich U-Zr alloys at temperatures below 880 K. In this work, a finite element method based mesoscale modeling technique is used to calculate the effective thermal conductivities of such heterogeneous microstructures, using the thermal conductivities of two individual phases and their interphase thermal resistance (Kapitza resistance) as input parameters. The Kapitza resistance between δ-UZr_2 and α-U is determined at different temperatures, which shows an approximately T^{-3} dependence in the temperature range between 300 K and 800 K. In addition, the Kapitza resistance exhibits a strong dependence on the aspect ratio of the δ-UZr_2 phase. An analytical model is therefore developed to quantify the effects of both temperature and δ-UZr_2 aspect ratio on the Kapitza resistance. Using this newly developed Kapitza resistance model, the effective thermal conductivities of a number of δ-UZr_2 + α-U heterogeneous microstructures in U-Zr alloys, including non-lamellar microstructures, can be estimated accurately.

Key words: Uranium-zirconium (U-Zr) metallic fuels; Effective thermal conductivity of heterogeneous microstructure; Kapitza resistance; Mesoscale modeling.

*Corresponding author. Email: xmbai@vt.edu (X.M. Bai)

1. Introduction

Uranium-zirconium (U-Zr) based metallic fuels are promising candidate nuclear fuels for next generation fast reactors [1]. In comparison with oxide fuels such as UO_2, U-Zr based metallic fuels typically have higher fissile density, higher thermal conductivity, and convenience for fuel recycling [1, 2]. However, metallic fuels are susceptible to fission-gas-induced fuel swelling as well as phase instability [1]. Like in oxide fuels, thermal transport properties such as thermal conductivity are critical for the metallic fuel performance because they are directly related to thermal energy conversion efficiency and fuel safety. For example, the effective fuel thermal conductivity determines the reactor fuel temperature and temperature gradient directly, which in turn affect fission gas induced swelling, fuel constituent redistribution, and phase decomposition [1, 3]. In general, a higher thermal conductivity is desired. However, fuel thermal conductivity degrades inevitably due to the microstructural evolution and radiation in the reactor environment [4]. Thus, it is crucial to understand and predict the effective thermal conductivity of metallic fuels under different circumstances, including the presence of various heterogeneous microstructures.

The U-Zr based metallic fuels are typically U-10wt.%Zr based fuels (commonly referred as U-10Zr. Note that unless specified differently, all compositions are based on weight percent in this paper). For example, U-10Zr and U-19Pu-10Zr fuels have been used in fast reactors such as Experimental Breeder Reactor II (EBR-II) [3, 5] and Fast Flux Test Facility (FFTF) reactor [6]. During service, the fuel rod center typically has a higher temperature than that at the rim region. Therefore, the metallic fuels experience significant constituent redistribution [7-10]. It has been found that in U-Zr based fuels, typically Zr migrates to the hot center region while U migrates to the intermediate region along the radial direction of a fuel rod [7, 8]. The constituent redistribution is due to the presence of both temperature gradient (Soret diffusion) and chemical potential gradient (Fickian diffusion) [9-11]. As a result, phase separation can occur in the fuel due to temperature variation (temperature gradient) and the inhomogeneous compositions along the radial direction of fuel rod [9-11]. For example, upon constituent redistribution, a U-10Zr fuel can have BCC γ phase (including both U-rich γ_1 and Zr-rich γ_2 phases [3]) of U-Zr solid solution in the hotter center region, γ-UZr + β-U at the intermediate region, and α-U + δ-UZr_2 at the colder rim region [7]. Even if without radiation, a U-10Zr alloy can form a microstructure with alternative lamellar α-U and δ-UZr_2 phases [12] at temperatures below the γ phase

transition temperature (~880 K) according to the phase diagram [13]. These phases have different physical properties including thermal conductivity. Therefore, it is important to predict the effective thermal conductivities of different heterogeneous microstructures in U-Zr fuels.

Previously, some semi-empirical, reduced-order thermal conductivity models have been developed to predict the average thermal conductivity of unirradiated U-Zr alloys if the nominal composition and the temperature are known [14-16]. For example, the present authors have developed a composition- and temperature-dependent thermal conductivity model for U-Zr alloys [14]. The model consists of a rule of mixture of the pure U and pure Zr thermal conductivities, as well as an additional mixing term to capture the alloying effect. The model parameters were calibrated using a subset of experimentally measured thermal conductivity data [17, 18]. Through comparing to many available experimental data (including those that were not included in the model fitting), the calibrated model can reasonably predict the average thermal conductivities of unirradiated U-Zr alloys at a wide range of temperatures (300 – 1200 K) and the whole composition range (from pure U to pure Zr) using a single set of parameters. Similarly, other reduced-order models [15, 16] can achieve comparable accuracies, as discussed in [14]. However, one drawback of these models is that they neglect the important microstructural information. As mentioned earlier, the microstructure evolution of U-Zr fuels in reactor environment is more complex than the unirradiated counterpart. As a result, the reduced-order models may not be sufficient because they ignore the effect of microstructures. Therefore, more accurate thermal conductivity models for U-Zr systems should take the microstructural information into account.

Regarding the microstructure-based thermal conductivity models, there are some early models (e.g., Maxwell-Garnett model [19, 20]) for estimating the effective thermal conductivities of heterogeneous composite or porous systems [19, 21]. These models are typically based on the rule of mixture (or inverse rule of mixture) but the effects of interface thermal resistance are typically ignored. However, Hasselman and Johnson [22] pointed out that the interfaces in composites should have nonzero interfacial thermal resistance. They derived an improved analytical model to explicitly include the interface thermal resistance effect in composite systems. Similarly, the interfaces between phases or grains in the same materials should also have a non-zero interface thermal resistance. Therefore, in the U-Zr fuels studied in

this work, the interface thermal resistance between different phases (e.g., α-U and δ-UZr_2) should not be overlooked, although it is unknown to date.

The interface thermal resistance is also called Kapitza resistance [23]. Due to the atomic-level or mesoscale discontinuity at the interface, a temperature drop (ΔT) is often observed across the interface when a heat flux (J) is applied. The Kapitza resistance is defined as $R = \Delta T / J$ according to Fourier's law. Therefore, Kapitza resistance can reduce the effective thermal conductivity. In many microstructure-based thermal conductivity modeling, the interface Kapitza resistance is often considered. For example, in UO_2 fuels with polycrystalline structures, the grain boundary Kapitza resistance is an important parameter for accurately predicting the effective thermal conductivity [24]. Millett et al. have used phase-field-based mesoscale modeling to calculate the effective Kapitza resistance for grain boundaries decorated with gas bubbles in UO_2 [25]. Similarly, Nan et al. [26, 27] have developed an effective thermal conductivity model for polycrystals and composites, which utilizes an effective medium approach combining the interface Kapitza resistance to calculate effective thermal conductivities. The model has been used by He et al. [28] for calculating the effective thermal conductivity of a two-phase polymer-matrix material. Badry and Ahmed [29] have used mesoscale modeling to study the interface thickness effect on the Kapitza resistance. By including this effect, the overall error of the predicted effective thermal conductivity was significantly reduced.

Kapitza resistance may change with temperature and interface morphology. As suggested by Pollack [23], Kapitza resistance shows a strong temperature dependence. Typically Kapitza resistance decreases with the increasing temperature (or equivalently, interface thermal conductance, which is the inverse of Kapitza resistance, increases with temperature) [23, 30], although an opposite trend was also reported [26]. For the interface morphologies, Millett et al. reported that the effective Kapitza resistance varies significantly with the grain boundary gas bubble morphologies in UO_2 [25]. However, many existing models [24, 27, 29] do not directly quantify the temperature effect as well as the geometry effect on the Kapitza resistance. Therefore, if a comprehensive Kapitza resistance model that directly quantifies the temperature and geometry (e.g., aspect ratio) effects is developed, the model can be applied to predict the effective thermal conductivities more accurately.

In this work, our focus is to develop a strategy to quantify the interphase Kapitza resistance in U-Zr systems, including both temperature and geometry dependences, using the lamellar interface between α-U and δ-UZr_2 phases as an example. To achieve this goal, a mesoscale modeling technique in the MOOSE (Multiphysics Object-Oriented Simulation Environment) framework [31] is used. MOOSE is an open-source partial differential equation solver based on the finite element method (FEM). MOOSE is also capable of generating the desired heterogeneous microstructures for this work. Using the mesoscale modeling, we have extracted the Kapitza resistances at different temperatures and for different geometries of the two phases. The obtained values are used to develop an analytical model to capture the effects of both temperature and geometry effects on the interphase Kapitza resistance between α-U/δ-UZr_2 phases. Coupling this new Kapitza resistance model with the mesoscale modeling, we can accurately predict the effective thermal conductivities of different α-U + δ-UZr_2 lamellar and circular structures in U-Zr fuels at a wide range of temperatures. Although this work only focuses on the α-U/δ-UZr_2 interphase Kapitza resistance, the methodology may be extended to other interface systems.

2. Simulation methods

2.1. Method for determine the interphase Kapitza resistance

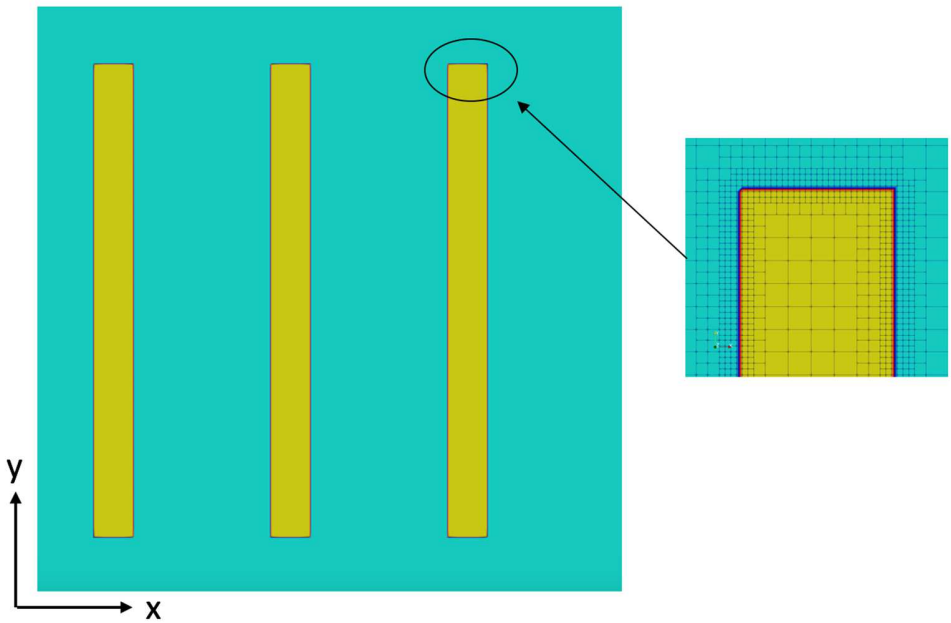

(a) (b)

Fig. 1. (a) Constructed microstructure in MOOSE with lamellar δ-UZr_2 precipitates embedded in an α-U matrix. (b) The magnified view of the adaptive meshes near the α-U/δ-UZr_2 interface. Yellow: δ-UZr_2; Cyan: α-U. Purple: δ-UZr_2/ α-U interface.

As mentioned earlier, we use finite-element-method (FEM) based mesoscale modeling in the MOOSE framework [31] to predict the effective thermal conductivity of U-rich U-Zr systems, in which the predominant microstructure is α-U + δ-UZr_2 laminar structure when the temperature is below the γ-phase transition temperature [12, 13]. A representative 2-D laminar structure in our simulations is shown in Fig. 1(a), which contains lamellar δ-UZr_2 precipitates embedded in an α-U matrix with varying Zr weight fractions. The aspect ratio of δ-UZr_2 is defined as its length ratio in the longer (y direction) to the shorter (x direction).

To calculate the effective thermal conductivity of such a heterogeneous system, the thermal conductivities of the α-U and δ-UZr_2, as well as the interphase Kapitza resistance, should be provided as input parameters. The determination of these input parameters are described as follows. As mentioned earlier, our recently developed semi-empirical thermal conductivity model [14] can predict the thermal conductivities of U-Zr alloys at a wide range of temperature and the full range of alloy composition, including pure U. Therefore, in this work the thermal conductivity of pure U at a given temperature is predicted by our semi-empirical model. Figure 2 shows the good agreement between the prediction of our semi-empirical model [14] and the experimental data [17, 18] for pure U at different temperatures. For δ-UZr_2, however, there are only limited experimental data available until very recently in 2020 and 2021. Ding et al. have measured the thermal conductivity of UZr_2 at temperatures from 1.8 K to 300K [32]. Hua et al. have measured the thermal conductivity for U-50Zr at 296K [33]. The experimental value [33] at around 300 K is slightly lower than our model prediction, as shown in Fig. 2. The discrepancy is reasonable because δ-UZr_2 has a wide range of compositions or stoichiometries. According to the U-Zr phase diagram, the weight percentage of Zr in δ-UZr_2 can vary significantly, roughly from 40 – 60 wt.% [13, 34]. Due to the lack of experimental thermal conductivity data for δ-UZr_2 at temperatures above 300 K, we use our semi-empirical thermal conductivity model [14]

to predict its thermal conductivity between 300 K and 800 K, assuming that δ-UZr_2 has an ideal composition at U-43.4Zr.

However, the Kapitza resistance at the α-U/δ-UZr_2 interface is an unknown parameter. Therefore, initially it is a fitting parameter. Here we treat the interphase boundary as an additional "phase" with a local thermal conductivity (k_{int}) and a finite width d. Then the interphase Kapitza resistance (R) can be calculated:

$$R = d/k_{int}, \quad (1)$$

where d = 2.5 nm. To calibrate the Kapitza resistance, the calculated effective thermal conductivities of the heterogeneous system is fitted to the values predicted by our semi-empirical U-Zr thermal conductivity model [14] based on the nominal composition of the entire system. Here the thermal conductivities predicted by our semi-empirical U-Zr thermal conductivity model [14] are considered as "true values" or references because this model agrees with many available experimental data. Using this trial-and-error approach, the Kapitza resistance for α-U/δ-UZr_2 interphase boundary at different temperatures and aspect ratios can be determined. The determined Kapitza resistance values are used to fit an analytical model, as discussed in Section 3.3. Finally, the new analytical Kapitza resistance model is coupled with mesoscale modeling to predict effective thermal conductivities for other α-U + δ-UZr_2 microstructures (including non-lamellar microstructures) that are not included in the Kapitza resistance model fitting, as shown in Section 3.4.

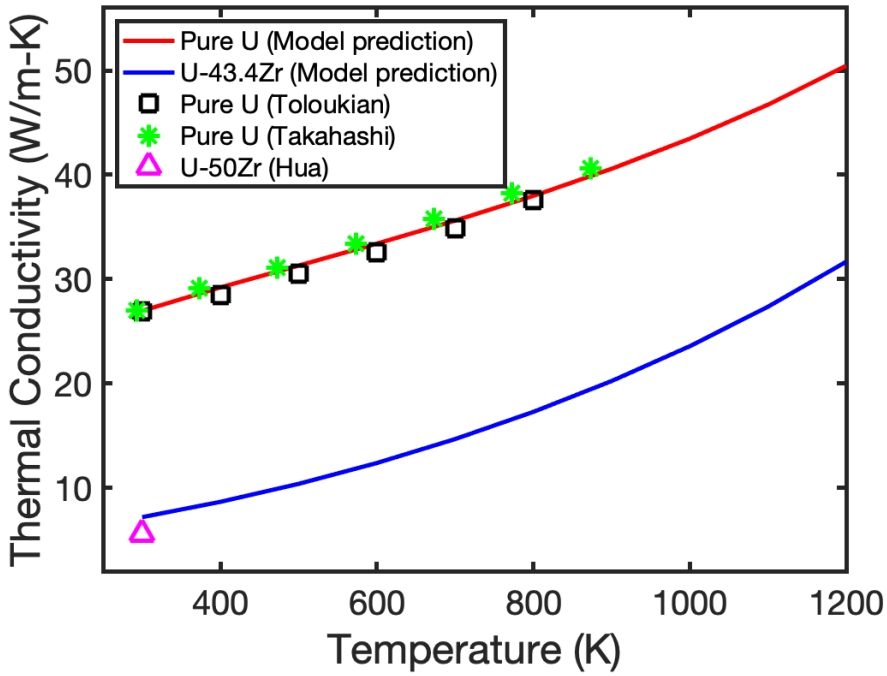

Fig. 2. The thermal conductivities of pure α-U and δ-UZr_2 as a function of temperature as predicted by our previous semi-empirical thermal conductivity model [14] (solid lines). The experimental data for pure α-U (open squares and filled asterisks) were collected or measured by Toloukian et al. [17] and Takahashi et al. [18]. The experimental data for δ-UZr_2 (open triangle) was measured by Hua et al. [33].

2.2. Details of mesoscale modeling using MOOSE

Here are some details of how to use a mesoscale modeling technique in the MOOSE framework [31] to calculate the effective thermal conductivity. For convenience, the phase field module in the MOOSE framework is used to model the heterogeneous microstructures. In the phase field method, the interface mobility is set to a very high value so that the interface remains sharp during the simulation. Therefore, our mesoscale modeling is essentially based on the FEM method. The dimensions of the simulation domain (Fig. 1(a)) are 1 μm × 1 μm. The Zr weight fraction varies from 5.2 ~ 13.4 wt.% (corresponding to 20 ~ 45% volume fraction of δ-UZr_2). The aspect ratio of δ-UZr_2 ranges from 5.4 to 12.15. The width of the α-U/δ-UZr_2 interphase

boundary is set to 2.5 nm, as mentioned earlier. The simulation temperature ranges between 300 K to 800 K, which is below the phase transition temperature of δ-UZr_2 to γ (~ 880 K [13]).

To calculate the effective thermal conductivity of the heterogeneous system, the heat conduction module can be used to impose a thermal gradient to the simulation system. After the system reaches the steady state, the effective thermal conductivity of the entire system can be calculated through Fourier's law. This is a direct method for calculating the effective thermal conductivity. However, in practice the direct method could induce some artifacts so that it is not used here. For example, as shown by Hales et al. [35], if some microstructural features are located at the simulation domain boundaries, the effective thermal conductivity calculated by the direct method may not be accurate. On the other hand, the asymptotic expansion homogenization (AEH) method [36-38] implemented in MOOSE can be used to solve such problems. The AEH method is capable of calculating the effective materials properties (e.g., thermal conductivity, elastic constants) through computing the microscopic properties at the mesoscale and intergrating them to obtain a homogenized (or effective) property over a periodic domain. In this work, the AEH method is actually used to calculate the effective thermal conductivities of heterogeneous microstructures. Note that A similar approach was also used to calculate the effective thermal conductivity in polycrystalline UO_2 systems containing xenon bubbles [24]. In the AEH method, a temperature gradient is also applied in each of the x and y directions in the 2-D simulation domain. In each direction, a thermal conductivity can be obtained by integrating the thermal conductivity at different mesh points. The final effective thermal conductivity reported here is obtained by averaging the thermal conductivities in the two directions. Therefore, the possibe orientation-dependent thermal conductivity shown in Fig. 1(a) is averaged out.

In FEM-based simulations, typically a finer mesh may give a more accurate result at the expense of computational efficiency. However, as demonstrated by Hales et al. [35], the AEH method does not necessarily require a very fine mesh to get accurate results. In addition, the mesh adaptivity is used in this work. The mesh adaptivity can adjust the mesh size automatically if needed (e.g., change to smaller mesh size at interphase boundaries). In this work, initially the simulation domain contains 100 meshes in each direction. After the mesh adaptivity is activated, the meshes near the interphase boundaries become finer. For example, Figure 1(b) shows a magnified view of the fine mesh at an interphase boundary generated by the mesh adaptivity.

2.3. 2D-3D thermal conductivity conversion

All the experimental data [17, 18] for U-Zr fuels were measured in 3D. Our semi-empirical, reduced-order analytical thermal conductivity model [14] was fitted to the 3D experimental data so that their predictions are also for 3D systems. However, the mesoscale modeling in this work is performed in 2D. If one thinks that the z direction in our simulations is infinite, the rectangular δ-UZr_2 domain in 2D (Fig. 1(a)) should correspond to a thin "sheet" or laminar structure in 3D. In this sense, it may be reasonable to use 2D simulations to model the laminar structures. However, in reality the laminar δ-UZr_2 phase may have different 3D orientations at different locations [12] so that the measured thermal conductivity is a 3-D averaged value. Therefore, the 2D thermal conductivity results calculated from mesoscale modeling should be converted to 3D in order to compare with the experimental data or the predictions from analytical models, and vice versa. Bakker [39] has developed an analytical model for the 2D-3D thermal conductivity conversion based on FEM modeling of heterogeneous systems contain dispersed phases such as porosity and inclusions. Teague et al. [40] have applied this model to convert the as-calculated 2D thermal conductivities to 3D values for mixed oxide (MOX) fuels. They validated the 2D - 3D conversion algorithm by comparing conversion results with the direct 3D mesoscale modeling results. The analytical equation is expressed as follows:

$$(1-(1-k_d/k_m)\emptyset_d - f_{2D}) = r(1-(1-k_d/k_m)\emptyset_d - f_{3D}) \quad (k_d < k_m), \tag{2}$$

$$r = 0.93 + \frac{1}{k_d/k_m + 1.03} \quad (k_d < k_m), \tag{3}$$

where k_d and k_m are the thermal conductivities for the second phase and the matrix, respectively; $\emptyset_d$ is the 2D volume fraction of the second phase; f_{2D} and f_{3D} are the fractions of the thermal conductivity with the second phase (heterogeneous structure) divided by the thermal conductivity without the second phase (pure matrix) for the 2D and 3D systems, respectively. Once f_{2D} is determined from 2D modeling, it can be converted to f_{3D} using Eqs. (2) and (3). Since the thermal conductivity of pure matrix (k_m) is known, the effective thermal conductivity of the heterogeneous structure in 3D can be obtained from $k_m \cdot f_{3D}$. Note that Eqs. (2) and (3) are valid only if $k_d < k_m$. In U-Zr fuels containing α-U + δ-UZr_2 microstructures, δ-UZr_2 is the

second phase while α-U is the matrix. At any given temperature, δ-UZr_2 always has a lower thermal conductivity than α-U, as shown in Fig. 2. Therefore, the $k_d < k_m$ condition is satisfied.

3. Results

3.1. Conversion of thermal conductivity between 3D and 2D

At first, we used the analytical equations (Eqs. (2) and (3)) developed by Bakker [39] to convert the 3D thermal conductivities of a U-10Zr alloy predicted by our semi-empirical U-Zr thermal conductivity model [14] to 2D values. The comparison between the 2D and 3D thermal conductivities for U-10Zr at different temperatures is shown in Fig. 3(a). Overall, the 2D thermal conductivities are slightly higher than the 3D thermal conductivities, which is in agreement with Bakker's results [39]. However, Teague's results [40] show that the 2D thermal conductivities are not necessarily higher than the 3D values. Nevertheless, the differences between 2D and 3D values in both Teague's work [40] and this work are small (< 6%).

Similar to Badry's [41] approach, an error rate E_{err} is used to quantify such difference, which is defined as:

$$E_{err} = \frac{k_{3D} - k_{2D}}{k_{3D}}, \quad (4)$$

where k_{3D} is the 3D thermal conductivity predicted by our semi-empirical model [14], k_{2D} is the converted 2D thermal conductivity. Figure 3(b) shows the error between the converted-2D and 3D thermal conductivities for U-Zr alloys with δ-UZr_2 volume fraction ranging from 10% to 40% (corresponding to Zr weight fraction from 2.49 – 11.61 wt.%). The error gradually increases with the increasing δ-UZr_2 volume fraction, which is consistent with the simulation results from Badry et al. [41]. According to Badry et al. [41], such an increase in error is reasonable since it depends on the morphology and distribution of the second phase. Although in general the error between 2D and 3D thermal conductivities is small, the thermal conductivities predicted by our semi-empirical model [14] are still converted into the 2D values to have an unambiguous comparison with the results from 2D mesoscale modeling.

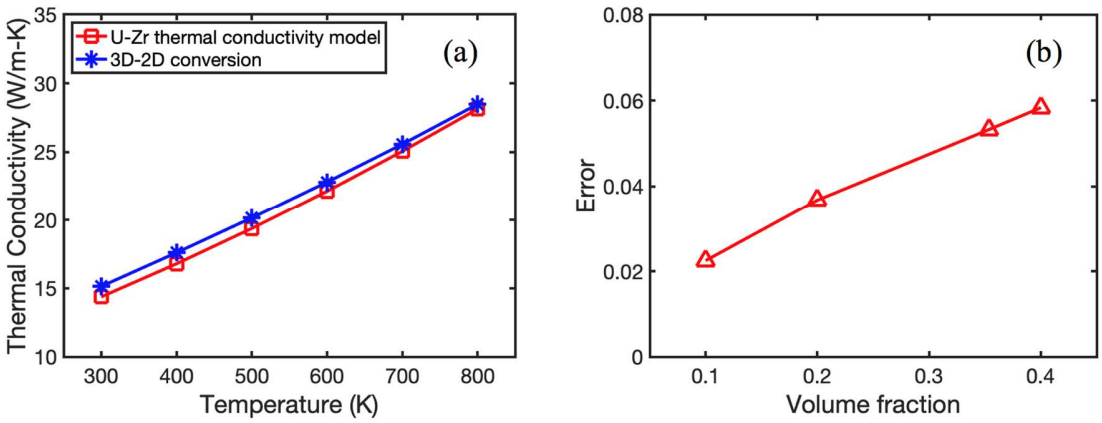

Fig. 3. (a) Comparison between 3D and converted-2D U-10Zr thermal conductivities as a function of temperature. The 3D thermal conductivities are predicted by our semi-empirical thermal conductivity model [14]. (b). The error between 3D and converted-2D thermal conductivities at 300 K as a function of δ-UZr_2 volume fraction (for U-Zr alloys with 2.49 – 11.61 wt.% Zr).

3.2. Effective thermal conductivity without Kapitza resistance

To demonstrate the importance of interphase Kapitza resistance, first Kapitza resistance is ignored in our mesocale modeling for calculating the effective thermal conductivities of lamellar α-U + δ-UZr_2 microstructures. Here the U-10Zr is used as an example, in which the δ-UZr_2 volume fraction is 35.4% and the aspect ratio of δ-UZr_2 is fixed at 8.1. The temperature-dependent thermal conductivities of both α-U and δ-UZr_2 are extrapolated from our semi-empirical U-Zr thermal conductivity model [14], as shown in Fig. 2. In Fig. 4, the calculated effective thermal conductivity as a function of temperature from the mesoscale modeling is compared with our semi-empirical U-Zr thermal conductivity model [14]. Again the thermal conductivities predicted by our semi-empirical model [14] are considered as "true values" or references because this model agrees with many experimental data. It can be clearly seen that the discrepancy is large between the mesoscale modeling (when the Kapitza resistance is ignored) and the semi-empirical model, demonstrating the importance of Kapitza resistance.

We also compare our results with some analytical models in literature that are widely used to predict the effective thermal conductivity in composite or porous systems, as shown in Fig. 4. These models are: Maxwell-Garnett model [19, 20], Bruggeman model [21], and Hasselman-Johnson model [22]. These models are briefly described as follows. The Maxwell-Garnett model [19, 20] has the form:

$$k_{eff}^{Max} = 1 + \frac{3\emptyset_d}{\left(\frac{k_d+2k_m}{k_d-k_m}\right)-\emptyset_d}, \quad (5)$$

where k_m and k_d are the thermal conductivity for the α-U matrix and δ-UZr_2 phase respectively, and ϕ_d is the volume fraction for δ-UZr_2. The Bruggeman model [21] has the form:

$$k_{eff}^{Bru} = \frac{1}{4}\{A + (A^2 + 8k_m k_d)^{\frac{1}{2}}\}, \quad (6)$$

$$A = (3\phi_m - 1)k_m + (3\phi_d - 1)k_d, \quad (7)$$

where ϕ_m is the volume fraction of the matrix and all other parameters have the same meaning as in the Eq. (5). It should be noted that the above two models neglect the interphase Kapitza resistance. On the other hand, the Hasselman-Johnson (H-J) model [22] was developed to calculate the effective thermal conductivity by explicitly considering the interphase boundary thermal conductivity k_{int}, which can be expressed as:

$$k_{eff}^{H-J} = \frac{k_d}{\left(1-\frac{k_d}{k_m}+\frac{2k_d}{k_{int}}\right)\phi_d+\frac{k_d}{k_m}}, \quad (8)$$

where the local thermal conductivity at the interface is set to k_{int} = 1.5*W/K-m* at all temperatures in this work, and other parameters have the same meaning as in Eq. (5).

It can be seen in Fig. 4 that the Maxwell-Garnett model [19, 20] and Bruggeman model [21] are nearly identical, but they both overpredict the thermal conductivity at the full temperature range. The overprediction is also more pronounced than our mesoscale modeling. The overprediction by the two models is reasonable because they do not consider the interphase Kapitza resistance. However, the Hasselman-Johnson model [22], which uses a fixed interphase thermal conductivity (thus Kapitza resistance), slightly underpredicts the thermal conductivities, especially at low temperatures. The results again demonstrate that the α-U/δ-UZr_2 interphase Kapitza resistance should not be ignored. The results also suggest that the Kapitza resistance may be temperature-dependent, because Hasselman-Johnson model has a more underprediction

at higher temperatures when a fixed interphase thermal conductivity is used. Therefore, to accurately predict the effective thermal conductivities in mesoscale modeling, the α-U/δ-UZr_2 interphase Kapitza resistance as well as its temperature dependence should be considered.

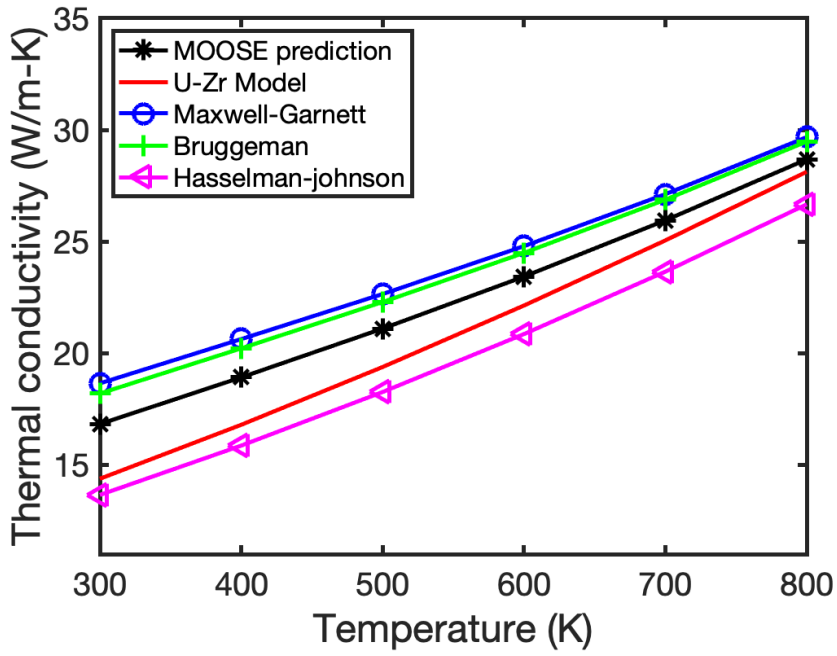

Fig. 4. Temperature-dependent thermal conductivities of U-10Zr predicted by different models. Note the average thermal conductivity predicted by our semi-empirical model [14] is used as the reference or true value here (red solid line). In the mesoscale modeling in MOOSE, a lamellar α-U + δ-UZr_2 microstructure is used, but the interphase Kapitza resistance is ignored. Other models are Maxwell-Garnett [19, 20], Bruggeman [21], Hasselman-Johnson [22].

3.3. Development of a Kapitza resistance model

As mentioned in the Method Section, the α-U/δ-UZr_2 interphase thermal conductivity (thus the Kapitza resistance) is first treated as a fitting parameter in our mesoscale modeling. During the fitting, the calculated effective thermal conductivities from the mesoscale modeling are fitted to our semi-empirical U-Zr thermal conductivity model [14]. To study the temperature dependence, the α-U/δ-UZr_2 interphase thermal conductivities in U-5.2Zr, U-8.3Zr and U-11.6Zr (in which the δ-UZr_2 volume fraction is 20%, 30%, 40%, respectively) are determined for

temperatures between 300 – 800 K. In all of these compositions, the δ-UZr_2 aspect ratio is fixed at 8.1. Once the interphase thermal conductivity is determined, the Kapitza resistance can be calculated using Eq. (1), where the interface thickness d = 2.5 nm. Figure 5(a) shows the calculated α-U/δ-UZr_2 interphase thermal conductivities as a function of temperature at the three δ-UZr_2 volume fractions. At these δ-UZr_2 volume fractions, the interphase thermal conductivity increases with the increasing temperature. At lower temperatures (< 600 K), the interphase thermal conductivity is not sensitive to the volume fraction. At higher temperatures (> 600 K), the interphase thermal conductivity is slightly larger for the smaller δ-UZr_2 volume fraction. Figure 5(b) shows the interphase Kapitza resistances as a function of temperature for the three δ-UZr_2 volume fractions, which is calculated from Fig. 5(a) using Eq. (1). The Kapitza resistance decreases with the increasing temperature for all δ-UZr_2 volume fractions. It should be noted that this temperature dependence behavior is consistent with many experimental results reported in literature [23, 30]. It increases slightly with δ-UZr_2 volume fraction at low temperatures (< 600K) but is insensitive to the δ-UZr_2 volume fraction at high temperatures (> 600 K). The results shown in Fig. 5(b) are reasonable because ideally Kapitza resistance should not depend on the volume fraction of the second phase. Overall, the Kapitza resistance is within a reasonable range between 0.1 – 5 m^2K/GW as temperature varies, which is in good agreement with the typical values (~ 2 m^2K/GW at room temperature) for metal-metal nanolaminate interface summarized by Liang et al. [42].

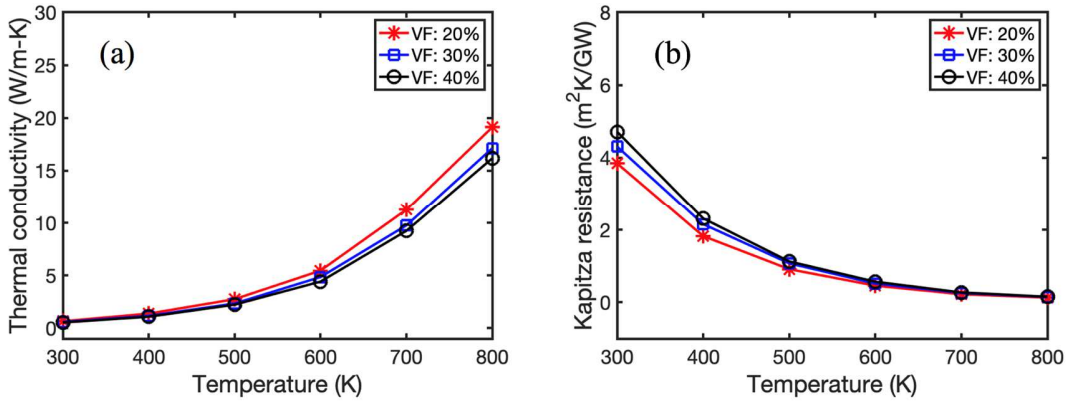

Fig. 5. Mesoscale modeling results of the temperature dependence on the α-U/δ-UZr_2 interphase thermal conductivities and Kapitza resistance for three U-Zr systems with δ-UZr_2 volume fraction (VF) at 20%, 30%, and 40% (representing U-5.2Zr, U-8.3Zr, and U-11.6Zr respectively). The δ-UZr_2 aspect ratio is fixed at 8.1. (a). Fitted α-U/δ-UZr_2 interphase thermal conductivities as a function of temperature for the three δ-UZr_2 volume fractions. (b) The corresponding α-U/δ-UZr_2 interphase Kapitza resistances as a function of temperature for the three δ-UZr_2 volume fractions.

Next, the effects of δ-UZr_2 aspect ratio and temperature on the Kapitza resistance are quantified. In this approach, the number of lamellar δ-UZr_2 in the α-U matrix is fixed but the aspect ratio of δ-UZr_2 is varied so that the volume fraction of δ-UZr_2 changes. The same fitting procedure discussed above is used to obtain the Kapitza resistances for different aspect ratios and temperatures. As discussed in literature [23, 43-46], the Kapitza resistance has a T^{-3} dependence. The general expression for Kapitza resistance derived by Khater and Szeftel [44] has the form,

$$RT^3 = \frac{\beta^3\left(1+8\beta^{-1}\right)^{-1}}{2\varepsilon C d}\frac{1}{2\Theta_h^2+T\Theta_h\partial\Theta_h/\partial T}, \qquad (9)$$

where R is the Kapitza resistance, β is a statistical term, ε is the flatness of the interface, d is the atomic layer thickness, Θ_h is the Debye temperature, C is a material related parameter and $\partial\Theta_h/\partial T$ is the first-order derivative of Debye temperature with temperature. It has been shown that $\partial\Theta_h/\partial T$ is zero at temperatures below the Debye temperature so that the Kapitza resistance has a clear T^{-3} dependence [23, 43-46]. For temperatures above the Debye temperature, $\partial\Theta_h/\partial T$ is nonzero so that the value of RT^3 is typically smaller. For α-U, the Debye temperature is around 280 K from density functional theory modeling [47]. Ren et al. [47] used the Quasi-harmonic Debye model [48] to calculate $\partial\Theta_h/\partial T$ for α-U between 0 - 900 K and found that it is negligible. Therefore, $\partial\Theta_h/\partial T$ may be assumed to be zero and Eq. (9) can be re-written as:

$$RT^3 = \frac{\beta^3\left(1+8\beta^{-1}\right)^{-1}}{2\varepsilon C d}\frac{1}{2\Theta_h^2}. \qquad (10)$$

In this case, the Kapitza resistance has a T^{-3} dependence if the right-hand side of Eq. (10) can be approximated as a constant. Therefore, Equation (10) is simply written as,

$$RT^3 = B, \qquad (11)$$

where B is assumed to be a constant.

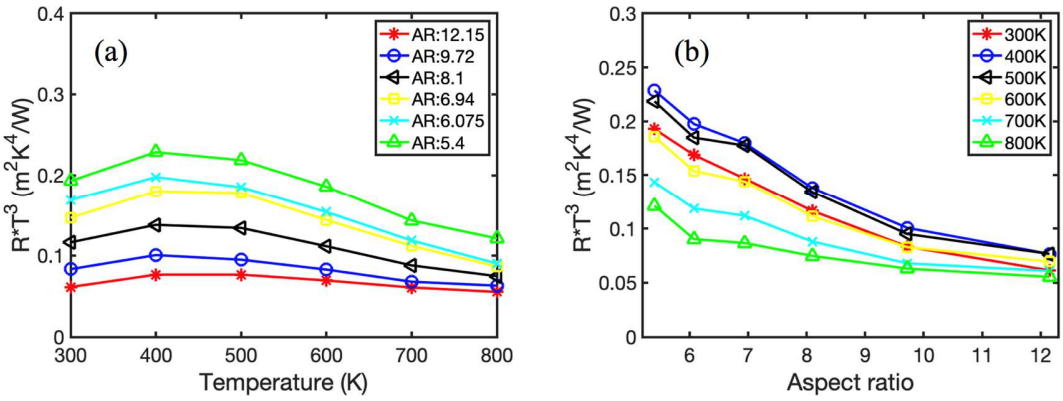

Fig. 6. (a) RT^3 as a function of temperature for α-U + δ-UZr_2 laminar structure with fixed number of δ-UZr_2 but varying δ-UZr_2 aspect ratio ranging from 5.4 to 12.15. (b) RT^3 as a function of aspect ratio at different temperatures. Note that the vertical axis in (b) has a smaller scale than in (a).

To quantify the effects of both temperature and δ-UZr_2 aspect ratio on the Kapitza resistance, we calculated R for δ-UZr_2 volume fraction ranging from 20% to 45% (representing U-5.2Zr to U-13.44Zr) at different temperatures (300 – 800 K) and varying δ-UZr_2 aspect ratios (5.4 – 12.15). The RT^3 as a function of temperature as well as the δ-UZr_2 aspect ratio is shown in Fig. 6. In Fig. 6(a), when the aspect ratio of δ-UZr_2 is above 8.1, RT^3 only varies slightly with temperature, which agrees well with Eq. (11) that the Kapitza resistance has a nearly T^{-3} dependence. For smaller δ-UZr_2 aspect ratios (< 8.1), initially RT^3 increases slightly then decreases with the increasing temperature. According to Eq. (9), above the Debye temperature, even though the value of $\partial\Theta_h/\partial T$ is small, it may still impact the overall value of RT^3. Therefore, the slight decrease in RT^3 at higher temperatures is reasonable. Overall, the Kapitza resistance fluctuates slightly with temperature at a given aspect ratio. In terms of δ-UZr_2 aspect ratio dependence, RT^3 decreases almost monotonically with increasing aspect ratio at all temperatures, as shown in Fig. 6(b). The slope for RT^3 is similar at temperatures between 300 and 600K, but is smaller at 700 K and 800 K. This is because the Kapitza resistance decreases at high temperatures, as shown in Fig. 5(b). Based on our mesoscale modeling results, we approximate

that the interphase Kapitza resistance has a roughly T^{-3} dependence (especially at high aspect ratios), while it has a strong dependence on the δ-UZr_2 aspect ratio.

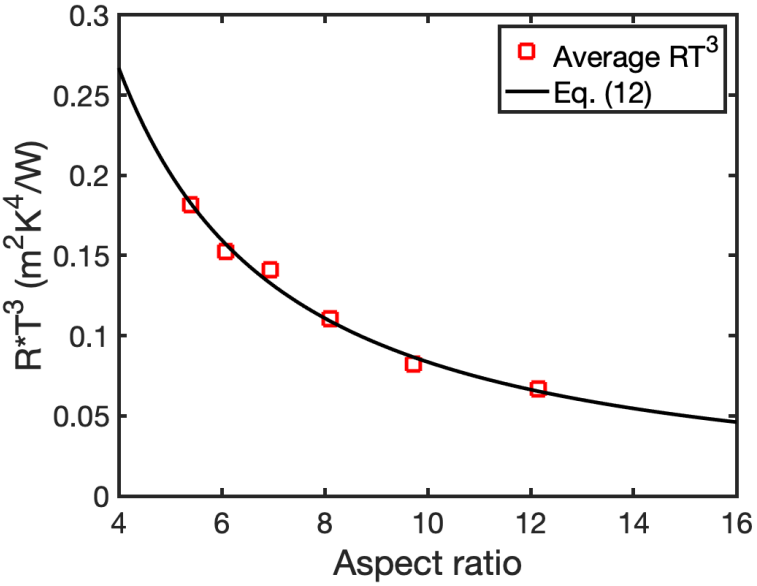

Fig. 7. Comparison between the averaged RT^3 (open squares) over the full temperature range (300 – 800 K) and the fitted Kapitza resistance model (Eq. (12), solid line) as a function of δ-UZr_2 aspect ratio.

Since the Kapitza resistance has a roughly T^{-3} dependence, the average of RT^3 is obtained over the entire temperature range (300 – 800 K) for each δ-UZr_2 aspect ratio. The averaged RT^3 as a function of aspect ratio is shown in Fig. 7, which decreases with the increasing aspect ratio, and reaches a plateau when the aspect ratio is greater than 12. To include the effect of aspect ratio, Equation (11) is modified as,

$$RT^3 = a * (AR)^b, \qquad (12)$$

where AR is the aspect ratio of δ-UZr_2 phase; a and b are fitting parameters. Equation (12) is used to fit the averaged RT^3 values shown in Fig. 7, which gives a = 1.5463 and b = -1.267, respectively. Therefore, our new interphase Kapitiza resistance model (Eq. (12)) includes the effects of both temperature and δ-UZr_2 aspect ratio. This model will be used to predict the

effective thermal conductivities of different α-U + δ-UZr_2 heterogeneous microstructures that are both within and out of the fitting range as discussed in the next section.

3.4. Effective thermal conductivity based on the new Kapitza resistance model

Finally, we implement Eq. (12) into MOOSE (denoted as R-MOOSE model) and use it to predict the effective thermal conductivities for U-Zr alloys consisting of α-U + δ-UZr_2 heterogeneous microstructures. The calculations are conducted both within and outside the fitting range to validate our newly developed temperature- and aspect-ratio-dependent Kapitza resistance model (Eq. (12)). Here "within the fitting range" means that both the δ-UZr_2 aspect ratio and Zr weight fraction are within the fitting range. In this work the fitting range for Zr weight percent is 5.22 – 13.44 wt.%, and that for the aspect ratio is 5.4 – 12.15. In our mesoscale modeling, the Kapitza resistance is predicted by Eq. (12), and thermal conductivities for α-U and δ-UZr_2 shown in Fig. 2 are also used as the input parameters. The effective thermal conductivities calculated by the R-MOOSE model is compared against our semi-empirical U-Zr thermal conductivity model [14], as shown in Fig. 8 for different U-Zr microstructures. Figure 8(a) shows the comparison when the U-Zr microstructure is within the fitting range, in which the composition is U-7.3Zr (δ-UZr_2 volume fraction at 27%) and the δ-UZr_2 aspect ratio is 9. As expected, the effective thermal conductivity predicted by the R-MOOSE model is in very good agreement with our semi-empirical U-Zr thermal conductivity model [14] at the full temperature range. In other three sub-figures, the comparisons are for U-Zr microstructures outside the fitting range. In Fig. 8(b), the δ-UZr_2 aspect ratio (AR = 15) is outside the fitting range while the composition U-9Zr (δ-UZr_2 volume fraction at 32.4%) is within the fitting range. The agreement is still very good. In Figs. 8(c) and 8(d), both of δ-UZr_2 aspect ratio and the Zr weight fraction are outside the fitting range. The microstructures are U-3.8Zr (δ-UZr_2 volume fraction at 15%) with δ-UZr_2 aspect ratio at 18 (Fig. 8(c)) and U-15.4Zr (δ-UZr_2 volume fraction at 50%) with δ-UZr_2 aspect ratio at 12.9 (Fig. 8(d)), respectively. The R-MOOSE model still accurately predicts the effective thermal conductivities for both microstructures.

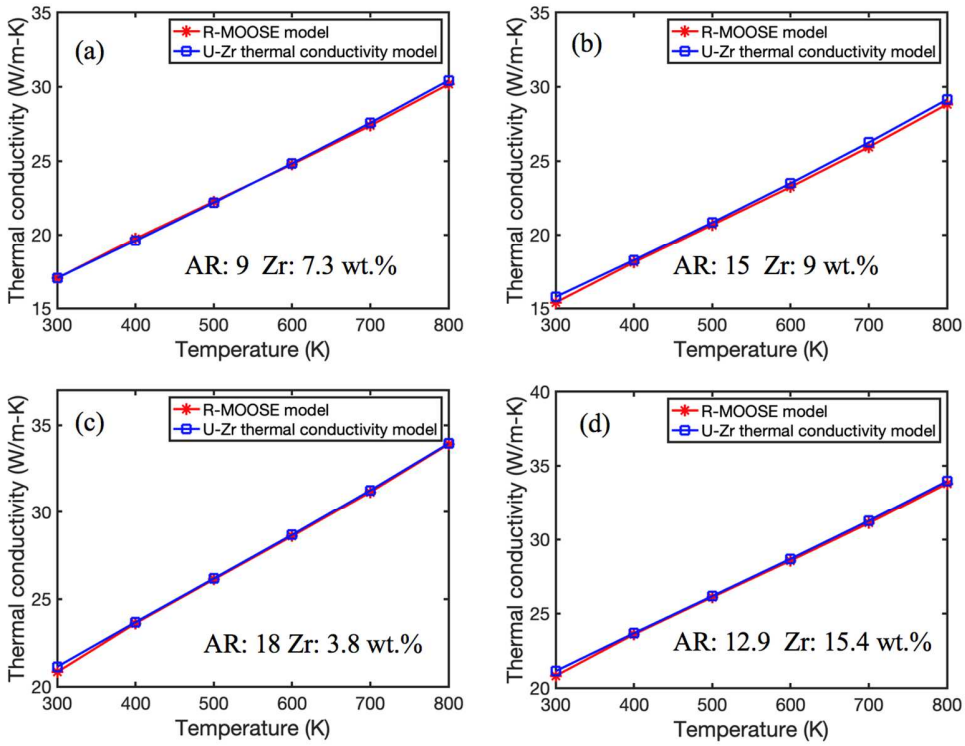

Fig. 8. Comparison between the R-MOOSE based mesoscale modeling and our semi-empirical U-Zr thermal conductivity model prediction [14] for different δ-UZr_2 aspect ratios and Zr weight fractions. (a) Within the fitting range, with δ-UZr_2 aspect ratio at 9 and Zr weight fraction at 7.3%. (b) Zr weight fraction within the fitting range at 9% but δ-UZr_2 aspect ratio outside of the fitting range at 15. (c). Both Zr weight fraction and aspect ratio outside of the fitting range at 3.8% and 18, respectively. (d) Both Zr weight fraction and aspect ratio outside of the fitting range at 15.4% and 12.9, respectively.

Although Figure 8 demonstrates that the R-MOOSE model can predict accurate effective thermal conductivity for the microstructures that are both within and out of the fitting range, the morphologies of these microstructures are rather simple. Specifically, the laminar δ-UZr_2 precipitates in each microstructure align in the same direction and of the same size. To test if the R-MOOSE model can be applied to more complex morphologies, two different microstructures are constructed. The first microstructure is shown in the inset of Fig. 9(a). In this case the

laminar δ-UZr_2 precipitates have both horizontal and vertical alignments. In addition, two sizes of laminar δ-UZr_2 precipitates are modeled: 0.7 μm × 0.1 μm and 0.35 μm × 0.05 μm. The aspect ratio is kept at 7 for both sizes. Overall, this microstructure corresponds to a U-6.55Zr alloy (δ-UZr_2 volume fraction = 0.245). Clearly, the mesoscale modeling based on our R-MOOSE model agrees very well with our semi-empirical U-Zr thermal conductivity model [14] over the entire temperature range. In the second microstructure, ten circular δ-UZr_2 precipitates with a radius of 0.1128 μm are modeled, as shown in the inset of Fig. 9(b). This microstructure corresponds to a U-11.6Zr alloy (δ-UZr_2 volume fraction = 0.4). Although the laminar δ-UZr_2 phase is frequently observed in unirradiated U-10Zr alloy [12], it has been reported that under neutron irradiation UZr_{2+x} phases can have complex microstructural evolution [49]. Therefore, we use this hypothetical microstructure to represent the non-laminar δ-UZr_2 under non-equilibrium conditions. For the circular δ-UZr_2, the aspect ratio is set to AR = 1 in Eq. (12). The interphase thickness is set to 10 nm for better convergence in this case while the Kaptiza resistance is still determined by Eqs. (1) and (12). As seen in Fig. 9(b), the agreement between the mesoscale R-MOOSE model and our semi-empirical model [14] is still very good over the entire temperature range. Therefore, for U-Zr microstructures both within and outside of the fitting range (Figs. 8 and 9), our R-MOOSE model consistently predicts accurate effective thermal conductivities at the entire applicable temperature range, demonstrating that this model is pretty robust.

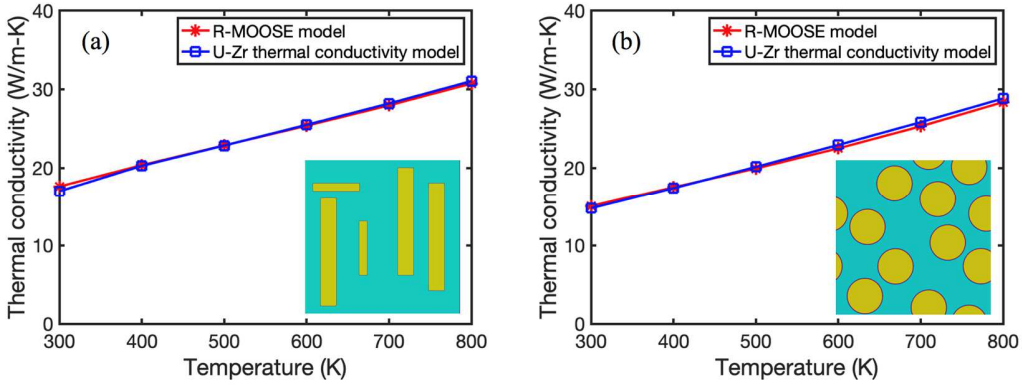

Fig. 9. Comparison between the R-MOOSE based mesoscale modeling and our semi-empirical U-Zr thermal conductivity model prediction [14] using two different microstructures. In the inset of each figure, yellow and cyan regions represent δ-UZr_2 precipitates and α-U matrix,

respectively. (a) Laminar δ-UZr_2 precipitates with different sizes and orientation alignments in a U-6.55Zr alloy. The aspect ratio is AR = 7 for both δ-UZr_2 sizes. (b) Circular δ-UZr_2 precipitates in a U-11.6Zr alloy. The aspect ratio is AR = 1.

4. Discussion

Although our interphase Kaptiza resistance model is based on α-U + δ-UZr_2 lamellar structures in U-Zr alloys, the methodology for determining the interphase Kapitza resistance could be extended to other interface systems. Our Kapitza resistance model assumes that RT^3 does not change significantly at temperatures above the Debye temperature for a given geometry. However, this is a rough assumption because RT^3 still varies with temperature, as shown in Fig. 6(a). If more sophisticated models can be developed to describe the temperature dependence of the Kapitza resistance, the transferability of the model may be further improved.

In this work, all the mesoscale simulations are conducted in 2-D. Although we have converted the 3-D experimental data (which are described by our semi-empirical U-Zr thermal conductivity model [14]) to 2-D values for a fair comparison, the conversion can introduce some errors, even though the errors could be small (Fig. 3). One limitation of 2-D simulations is that more complex combination of δ-UZr_2 orientations or spatial alignments cannot be captured. Therefore, it is unclear if our 2-D Kapitza resistance model can be seamlessly transferred to 3-D with a reasonable level of accuracy. To validate this transferability, independent 3-D simulations should be performed in the future.

The interphase Kaptiza resistance model developed in this work is based on unirradiated U-Zr alloys. In radiation environment, thermal conductivity can decrease significantly due to the irradiation effects [4]. If α-U + δ-UZr_2 heterogeneous microstructures can form in irradiated fuels (e.g., near the rim region), we envision that our Kaptiza resistance model might still be useful, given the fact that currently no other α-U/δ-UZr_2 interphase Kaptiza resistance model is available. However, the thermal conductivities of α-U and δ-UZr_2 phases should be replaced with the irradiated ones (although they are currently not available either to our best of knowledge). For other interphase boundaries that form during constituent redistribution, one could still use our α-U/δ-UZr_2 interphase Kaptiza resistance model as an approximation, because we expect that other interphase boundaries in U-Zr fuels would not have significantly different Kaptiza resistances

from α-U/δ-UZr_2 boundary. Therefore, this Kaptiza resistance model could be coupled with other models such as constituent redistribution model to predict microstructure-dependent thermal conductivity in U-Zr fuels during fuel performance modeling [15, 50].

However, U-Zr fuels can have more complex structural damage in reactor environment in addition to the constituent redistribution. Since α-U has an anisotropic swelling behavior due to its orthorhombic crystal structure, grain boundary tearing can occur in α-U near the low-temperature rim region [4, 10]. In addition, intergranular fission gas bubbles can form interconnected pores in α-U [4, 10]. As a result, high-conductivity bond sodium can infiltrate through these open channels [4]. The former two processes will reduce the effective thermal conductivity while the later will increase it [4]. These processes are not considered here as they are beyond the scope of this work. However, to accurately predict the effective thermal conductivities of U-Zr fuels in reactor environment, such important processes should not be overlooked.

5. Conclusions

In this work, mesoscale modeling coupled with the AEH method in the MOOSE framework has been used to calculate the effective thermal conductivities of U-Zr alloys containing α-U + δ-UZr_2 heterogeneous microstructures. The effective thermal conductivity is calculated basing on the thermal conductivity of each individual phase as well as the interface thermal resistance (Kapitza resistance) between them. Both Zr weight fraction and δ-UZr_2 aspect ratio are varied so that a variety of microstructures are modeled. The results are compared with our recently developed U-Zr thermal conductivity model [14], which is a semi-empirical, reduced-order model fitted to many experimental data. We found that if the α-U/δ-UZr_2 interphase boundary thermal resistance (or Kapitza resistance) is ignored, the effective thermal conductivities from the mesoscale modeling are over-predicted. Similar over-prediction is also found using some literature models [19, 21] in which the interphase Kapitza resistance is also not considered. Therefore, our results demonstrate that the α-U/δ-UZr_2 interphase Kapitza resistance should not be ignored in the microstructure-based mesoscale modeling.

To determine the α-U/δ-UZr_2 interphase Kapitza resistance, initially we treat it as a fitting parameter in our mesocale modeling. Different U-Zr heterogeneous microstructures with varying δ-UZr_2 volume fractions (thus the Zr weight fractions) and δ-UZr_2 aspect ratios are modeled. In addition, the mesoscale modeling is conducted at a wide range of temperatures (300 – 800 K). Our results show that the Kapitza resistance does not change much with the δ-UZr_2 volume fraction if the δ-UZr_2 aspect ratio is fixed. It is also found that the Kapitza resistance shows a roughly T^{-3} dependence for a given δ-UZr_2 aspect ratio, which is consistent with literature [23, 43-46]. Moreover, it is found that RT^3 decreases with increasing δ-UZr_2 aspect ratio. Using the Kapitza resistances extracted from the mesoscale modeling at different temperatures, aspect ratios, and δ-UZr_2 weight fractions, we have developed an analytical Kapitza resistance model to capture the effects of both temperature and aspect ratio of the second phase (δ-UZr_2) on the interphase Kapitza resistance.

After the temperature- and aspect-ratio-dependent Kapitza resistance model is calibrated, we implement it in the MOOSE (R-MOOSE) to calculate the effective thermal conductivities of heterogeneous U-Zr microstructures both within and outside the fitting range to validate the Kapitza resistance model. The R-MOOSE model accurately predicts the effective thermal conductivities of different U-Zr microstructures (including both laminar and circular δ-UZr_2 precipitates) at a wide range of temperatures and aspect ratios, demonstrating the robustness of this α-U/δ-UZr_2 interphase Kapitza resistance model. Using this model, it is possible to use meoscale modeling to predict the microstructure-dependent thermal conductivity in U-Zr alloys containing α-U + δ-UZr_2 heterogeneous microstructures if the temperature, aspect ratio, and thermal conductivities of individual phases are known. Although this work focuses on the α-U/δ-UZr_2 interphase Kapitza resistance, the methodology could be applied other interphase boundaries as well as the interfaces in other materials systems.

Acknowledgements

The authors thank the financial support from the U.S. Department of Energy, Nuclear Energy University Program (NEUP Award #DE-NE0008558) through Purdue University for initiating this work. X.M.B. also acknowledges his Startup fund and the Thomas G. Digges and

Thomas G. Digges Jr. Faculty Fellowship at Virginia Tech. The authors acknowledge the use of the computing facilities at the Advanced Research Computing (ARC) at Virginia Tech.

References

[1] T. Ogata, 3.01 - Metal Fuel A2 - Konings, Rudy J.M, Comprehensive Nuclear Materials, Elsevier, Oxford, 2012, pp. 1-40.
[2] T. Sofu, A review of inherent safety characteristics of metal alloy sodium-cooled fast reactor fuel against postulated accidents, Nuclear Engineering and Technology 47(3) (2015) 227-239.
[3] G.L. Hofman, R.G. Pahl, C.E. Lahm, D.L. Porter, Swelling behavior of U-Pu-Zr fuel, Metallurgical Transactions A 21(2) (1990) 517-528.
[4] T.H. Bauer, J.W. Holland, In-Pile Measurement of the Thermal Conductivity of Irradiated Metallic Fuel, Nuclear Technology 110(3) (1995) 407-421.
[5] R.D. Mariani, D.L. Porter, S.L. Hayes, J.R. Kennedy, Metallic Fuels: The EBR-II Legacy and Recent Advances, Procedia Chemistry 7 (2012) 513-520.
[6] W.J. Carmack, H.M. Chichester, D.L. Porter, D.W. Wootan, Metallography and fuel cladding chemical interaction in fast flux test facility irradiated metallic U-10Zr MFF-3 and MFF-5 fuel pins, J. Nucl. Mater. 473 (2016) 167-177.
[7] J.M. Harp, D.L. Porter, B.D. Miller, T.L. Trowbridge, W.J. Carmack, Scanning electron microscopy examination of a Fast Flux Test Facility irradiated U-10Zr fuel cross section clad with HT-9, J Nucl Mater 494 (2017) 227-239.
[8] Y.S. Kim, S.L. Hayes, G.L. Hofman, A.M. Yacout, Modeling of constituent redistribution in U-Pu-Zr metallic fuel, J Nucl Mater 359(1-2) (2006) 17-28.
[9] Y.S. Kim, G.L. Hofman, S.L. Hayes, Y.H. Sohn, Constituent redistribution in U–Pu–Zr fuel during irradiation, J. Nucl. Mater. 327(1) (2004) 27-36.
[10] J. Hirschhorn, M.R. Tonks, A. Aitkaliyeva, C. Adkins, A study of constituent redistribution in U–Zr fuels using quantitative phase-field modeling and sensitivity analysis, J. Nucl. Mater. 523 (2019) 143-156.
[11] G.L. Hofman, S.L. Hayes, M.C. Petri, Temperature gradient driven constituent redistribution in U・Zr alloys, J. Nucl. Mater. 227(3) (1996) 277-286.
[12] J.T. McKeown, S. Irukuvarghula, S. Ahn, M.A. Wall, L.L. Hsiung, S. McDeavitt, P.E.A. Turchi, Coexistence of the α and δ phases in an as-cast uranium-rich U–Zr alloy, J Nucl Mater 436(1) (2013) 100-104.
[13] M. Kurata, T. Ogata, K. Nakamura, T. Ogawa, Thermodynamic assessment of the Fe–U, U–Zr and Fe–U–Zr systems, Journal of Alloys and Compounds 271-273 (1998) 636-640.
[14] W. Chen, X.-M. Bai, Temperature and composition dependent thermal conductivity model for U-Zr alloys, J. Nucl. Mater. 507 (2018) 360-370.
[15] J. Hales, R. Williamson, S. Novascone, G. Pastore, B. Spencer, D. Stafford, K. Gamble, D. Perez, W. Liu, BISON Theory Manual The Equations Behind Nuclear Fuel Analysis, Idaho National Laboratory (INL), Idaho Falls, ID (United States), 2016.
[16] Y.S. Kim, T.W. Cho, D.S. Sohn, Thermal conductivities of actinides (U, Pu, Np, Cm, Am) and uranium-alloys (U-Zr, U-Pu-Zr and U-Pu-TRU-Zr), J Nucl Mater 445(1-3) (2014) 272-280.
[17] Y. Touloukian, P. Powell, C. Ho, P. Klemens, Thermodynamics properties of matter, Vol. 1, Plenum, New York, 1970.
[18] Y. Takahashi, M. Yamawaki, K. Yamamoto, Thermo-Physical Properties of Uranium Zirconium Alloys, J Nucl Mater 154(1) (1988) 141-144.
[19] J.C. Maxwell, A treatise on electricity and magnetism, vol. I, 3rd Ed, Oxford University Press (1904).
[20] J.C.M. Garnett, J. Larmor, XII. Colours in metal glasses and in metallic films, Philosophical Transactions of the Royal Society of London. Series A, Containing Papers of a Mathematical or Physical Character 203(359-371) (1904) 385-420.

[21] D.A.G. Bruggeman, Berechnung verschiedener physikalischer Konstanten von heterogenen Substanzen. I. Dielektrizitätskonstanten und Leitfähigkeiten der Mischkörper aus isotropen Substanzen, Annalen der Physik 416(7) (1935) 636-664.
[22] D.P.H. Hasselman, L.F. Johnson, Effective Thermal Conductivity of Composites with Interfacial Thermal Barrier Resistance, Journal of Composite Materials 21(6) (1987) 508-515.
[23] G.L. Pollack, Kapitza Resistance, Reviews of Modern Physics 41(1) (1969) 48-81.
[24] X.-M. Bai, M.R. Tonks, Y. Zhang, J.D. Hales, Multiscale modeling of thermal conductivity of high burnup structures in UO2 fuels, J. Nucl. Mater. 470 (2016) 208-215.
[25] P.C. Millett, M.R. Tonks, K. Chockalingam, Y. Zhang, S.B. Biner, Three dimensional calculations of the effective Kapitza resistance of UO2 grain boundaries containing intergranular bubbles, J. Nucl. Mater. 439(1) (2013) 117-122.
[26] C.-W. Nan, R. Birringer, Determining the Kapitza resistance and the thermal conductivity of polycrystals: A simple model, Phys Rev B 57(14) (1998) 8264-8268.
[27] C.-W. Nan, R. Birringer, D.R. Clarke, H. Gleiter, Effective thermal conductivity of particulate composites with interfacial thermal resistance, Journal of Applied Physics 81(10) (1997) 6692-6699.
[28] B. He, B. Mortazavi, X. Zhuang, T. Rabczuk, Modeling Kapitza resistance of two-phase composite material, Composite Structures 152 (2016) 939-946.
[29] F. Badry, K. Ahmed, A new model for the effective thermal conductivity of polycrystalline solids, AIP Advances 10(10) (2020) 105021.
[30] H.-K. Lyeo, D.G. Cahill, Thermal conductance of interfaces between highly dissimilar materials, Phys. Rev. B 73(14) (2006) 144301.
[31] D. Gaston, C. Newman, G. Hansen, D. Lebrun-Grandié, MOOSE: A parallel computational framework for coupled systems of nonlinear equations, Nuclear Engineering and Design 239(10) (2009) 1768-1778.
[32] X. Ding, T. Yao, L. Fu, Z. Hua, J. Harp, C. Marianetti, M. Neupane, M.E. Manley, D. Hurley, K. Gofryk, Magnetic, transport and thermal properties of δ-phase UZr2, Philosophical Magazine Letters 101(1) (2021) 1-11.
[33] Z. Hua, T. Yao, A. Khanolkar, X. Ding, K. Gofryk, L. He, M. Benson, D. Hurley, Intragranular thermal transport in U–50Zr, J. Nucl. Mater. 534 (2020) 152145.
[34] R.I. Sheldon, D.E. Peterson, The U-Zr (Uranium-Zirconium) system, Bulletin of Alloy Phase Diagrams 10(2) (1989) 165-171.
[35] J.D. Hales, M.R. Tonks, K. Chockalingam, D.M. Perez, S.R. Novascone, B.W. Spencer, R.L. Williamson, Asymptotic expansion homogenization for multiscale nuclear fuel analysis, Computational Materials Science 99 (2015) 290-297.
[36] P.W. Chung, K.K. Tamma, R.R. Namburu, Homogenization of Temperature-Dependent Thermal Conductivity in Composite Materials, Journal of Thermophysics and Heat Transfer 15(1) (2001) 10-17.
[37] Y.S. Song, J.R. Youn, Evaluation of effective thermal conductivity for carbon nanotube/polymer composites using control volume finite element method, Carbon 44(4) (2006) 710-717.
[38] V.V. Jikov, S.M. Kozlov, O.A. Oleinik, Homogenization of differential operators and integral functionals, Springer Berlin Heidelberg,1994.
[39] K. Bakker, Using the finite element method to compute the influence of complex porosity and inclusion structures on the thermal and electrical conductivity, International Journal of Heat and Mass Transfer 40(15) (1997) 3503-3511.
[40] M.C. Teague, B.S. Fromm, M.R. Tonks, D.P. Field, Using Coupled Mesoscale Experiments and Simulations to Investigate High Burn-Up Oxide Fuel Thermal Conductivity, JOM 66(12) (2014) 2569-2577.
[41] F. Badry, R. Brito, M.G. Abdoelatef, S. McDeavitt, K. Ahmed, An Experimentally Validated Mesoscale Model of Thermal Conductivity of a UO2 and BeO Composite Nuclear Fuel, JOM 71(12) (2019) 4829-4838.

[42] X. Liang, M. Baram, D.R. Clarke, Thermal (Kapitza) resistance of interfaces in compositional dependent ZnO-In2O3 superlattices, Applied Physics Letters 102(22) (2013) 223903.
[43] H. Haug, K. Weiss, A modified theory of the Kapitza resistance, Physics Letters A 40(1) (1972) 19-21.
[44] A. Khater, J. Szeftel, Theory of the Kapitza resistance, Phys Rev B 35(13) (1987) 6749-6755.
[45] A.C. Anderson, W.L. Johnson, The Kapitza resistance between copper and3He, Journal of Low Temperature Physics 7(1) (1972) 1-21.
[46] J.-L. Barrat, F. Chiaruttini, Kapitza resistance at the liquid—solid interface, Molecular Physics 101(11) (2003) 1605-1610.
[47] Z. Ren, J. Wu, R. Ma, G. Hu, C. Luo, Thermodynamic properties of α-uranium, J Nucl Mater 480 (2016) 80-87.
[48] M.A. Blanco, E. Francisco, V. Luaña, GIBBS: isothermal-isobaric thermodynamics of solids from energy curves using a quasi-harmonic Debye model, Computer Physics Communications 158(1) (2004) 57-72.
[49] T. Yao, L. Capriotti, J.M. Harp, X. Liu, Y. Wang, F. Teng, D.J. Murray, A.J. Winston, J. Gan, M.T. Benson, L. He, α-U and ω-UZr2 in neutron irradiated U-10Zr annular metallic fuel, J. Nucl. Mater. 542 (2020) 152536.
[50] M.R. Tonks, D. Gaston, P.C. Millett, D. Andrs, P. Talbot, An object-oriented finite element framework for multiphysics phase field simulations, Computational Materials Science 51(1) (2012) 20-29.